Journal of Petroleum Science and Engineering 208 (2022) 109792

Contents lists available at ScienceDirect

Journal of Petroleum Science and Engineering

journal homepage: www.elsevier.com/locate/petrol

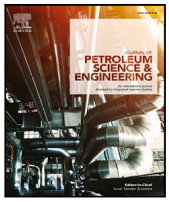

Restoration of annular zonal isolation using localized casing expansion (LCE) technology: Treatment of near-horizontal test sections containing a free-water channel

K. Beltrán-Jiménez [a], H.J. Skadsem [b,a,*], J.K. Sunde [a], D. Gardner [a], T.K.T. Wolterbeek [c], E.K. Cornelissen [d], W.J.G. Keultjes [d]

[a] Norwegian Research Centre AS, P.O. Box 8046, 4068 Stavanger, Norway
[b] University of Stavanger, P.O. Box 8600, 4036 Stavanger, Norway
[c] HPT Laboratory, Department of Earth Sciences, Utrecht University, Princetonlaan 4, 3584CB Utrecht, The Netherlands
[d] Wells Technology, Shell Global Solutions International B. V., Grasweg 31, 1031HW Amsterdam, The Netherlands

ARTICLE INFO

Keywords:
Well integrity
Well abandonment
Sustained casing pressure
Surface casing vent flow
Annular fluid migration
Casing expansion

ABSTRACT

Fluid migration behind casings is a well integrity problem that can result in sustained casing pressure, undetected leaks to the environment, and potentially very difficult remediation attempts. Traditional methods for treating annular fluid migration are perf-and-squeeze cementing or section milling followed by recementing. The main disadvantage of the former is the limited penetrability of cement slurry into narrow cracks and microannuli, while for the latter it is the requirement of a full rig to perform the operation. Casing expansion is a recent alternative remediation technology that involves imposing a permanent radial expansion of the casing and external cement layer, with the purpose of mechanically closing pathways for migrating fluids. A necessary requirement for the treatment to be effective is that the annular cement is confined between casings or between casing and competent rock formations, such that the cement can sustain significant mechanical strains without failure. Recent laboratory experiments and field trials have shown casing expansion to be a promising alternative to traditional treatment methods. We build on these insights and perform controlled treatment experiments involving a 7-in Local Expander tool and full-scale cemented annulus test assemblies, which contained much larger-scale defects than previously tested. Prior to treatment, the test assemblies had continuous migration channels on the top side of the cement, leading to high effective permeabilities ranging from approximately 80 to hundreds of darcy. The origin of the defects was likely separation of free water from the cement slurry, which is considered a relevant failure mode for primary cementing of inclined wellbores. We study the effect of imposing single and multiple local dents on the annular seepage rates, and probe for potential alteration of the cement and casing properties using Vickers hardness testing. We find that casing expansion can be highly effective in treating relatively major defects in cemented annuli, even when the defect is several millimeters wide and located adjacent to the outer casing. The effectiveness of the treatment is found to be linked to the degree of casing expansion and the initial condition of the annular cement. The deformed cement shows a tendency toward increased Vickers hardness, which is likely linked to densification of the cement microstructure. Vickers hardness testing of casing steel indicated no significant changes in hardness at the dent locations compared to average hardness values away from these points.

1. Introduction

Whether for conventional hydrocarbon production or for emerging uses of the subsurface, such as geothermal energy production or geological CO_2 sequestration, wellbores are drilled through layers of rock formations and penetrate natural barriers in the form of low permeable zones. To prevent uncontrolled cross-flow of formation fluids along the wellbore, casing strings or liners are run in the hole and cemented to the formation in an operation known as primary cementing (Nelson and Guillot, 2006). During primary cementing, drilling fluid is displaced from the annular space behind the casing or liner to be cemented and replaced by a cement slurry that hardens into a solid cement sheath. Important functions of the cement include ensuring zonal isolation

* Corresponding author at: University of Stavanger, P.O. Box 8600, 4036 Stavanger, Norway.
E-mail address: hans.j.skadsem@uis.no (H.J. Skadsem).

https://doi.org/10.1016/j.petrol.2021.109792
Received 21 July 2021; Received in revised form 31 October 2021; Accepted 1 November 2021
Available online 14 November 2021

along the annulus, providing mechanical support for the casing, and preventing contact between formation fluids and the cemented casing string or liner (Nelson and Guillot, 2006). Failure to isolate the annulus hydraulically can result in seepage of formation fluids past the cement and into other permeable formations or to the surface, where it often results in sustained casing pressure (SCP).

Annular fluid migration is a key industrial challenge, partly due to the challenges associated with remediation, and partly due to the safety, environmental and economic consequences of untreated wells, including seepage of formation fluids to the environment and contamination of potable groundwater. Of approximately 15,500 producing, shut-in and temporarily abandoned wells on the outer continental shelf of the Gulf of Mexico (period 1973 to 2003), 43% exhibited SCP on at least one casing annulus (Brufatto et al., 2003). Watson and Bachu (2009) found surface vent flow or gas migration outside casing in 15.5% of the examined onshore wells in an area of Alberta, Canada (Watson and Bachu, 2009). In a pilot study based on wells on the Norwegian Continental Shelf, Vignes and Aadnøy (2010) found well integrity failures, issues or uncertainties in as many as 18% of the 406 wells examined in the study (Vignes and Aadnøy, 2010). A comprehensive overview of published statistics related to well barrier and well integrity failures, including those mentioned above, is provided by Davies et al. (2014).

Poor annular cement is one of the most common causes of SCP. Several mechanisms can compromise the integrity of the cement, such as incomplete drilling fluid displacement during cementing (McLean et al., 1967; Bittleston and Guillot, 1991; Nelson and Guillot, 2006), gas migration as the cement is about to set (Carter and Slagle, 1972; Tao et al., 2021) and cement shrinkage during curing (Parcevaux and Sault, 1984; Sabins and Sutton, 1991; Justnes et al., 1995; Wolterbeek et al., 2021a). Required pressure testing of casings and formation below the newly set cement, as well as pressure and temperature variations experienced during production generate mechanical stresses that potentially result in fractures or debonding and loss of zonal isolation (Goodwin and Crook, 1992; Jackson and Murphey, 1993; Zhang and Bachu, 2011; Bois et al., 2011). Although the main mechanisms responsible for loss of zonal isolation appear to be relatively well understood by now, remediation of annular migrations paths is still a major challenge for the industry.

Conventional treatment of SCP often involves an expensive workover rig for perforating the casing followed by squeeze cementing of the annulus showing SCP, hoping that the cement will plug annular leakage paths. Experience indicates low success rates for such squeeze cementing operations, exemplified by a study of 137 operations carried out in the period 1992–2000 in an aging West Texas field (Cowan, 2007). Only about 34% of the squeeze operations were successful on the first attempt, and among the wells where the first attempt failed, the overall success rate did not exceed 60% with repeated squeeze operations (Cowan, 2007). Other conventional approaches to annulus remediation include cutting and pulling or section milling of the casing, followed by recementing.

Casing expansion offers an entirely different remediation approach, which does not require perforating or cutting and pulling the casing. Instead, casing expansion relies on the observation that confined cement can withstand mechanical strains of several percent without failing (Nelson and Guillot, 2006; Handin, 1965; Sakai et al., 2016). The technology is based on mechanical expansion of the inner casing, which in turn displaces and compresses the annular cement to potentially close migration paths (Kupresan et al., 2014; Du et al., 2015; Radonjic et al., 2015; Wolterbeek et al., 2021b). In the study by Kupresan et al. (2014), the casing expansion was studied in short annulus sections consisting of 2 3/8 in pipes cemented inside 4 in pipes (Kupresan et al., 2014). The cemented annuli had initial permeabilities in the order 0.1–10 darcy. Upon radially expanding the inner pipe by 2%–8% using an expansion cone, the permeability of the annulus was found to reduce by several orders of magnitude. Post-test, inspection of the compressed cement suggested compaction due to pore collapse, displacement of pore fluid, and a softening and rehydration of the cement (Kupresan et al., 2014; Radonjic and Kupresan, 2014).

The study of Kupresan et al. (2014) and Radonjic and Kupresan (2014) demonstrated the potential of using casing expansion to remedy annular fluid migration. A wireline-deployable tool implementation of this concept has been developed by Cornelissen (2019). This "Local Expander" tool imposes a *localized* casing expansion (LCE) where multiple hardened steel fingers are driven into the wall of the inner casing to produce plastic deformation of the casing and compression of the annular cement outside the casing (Wolterbeek et al., 2021b). Extensive laboratory studies of casing expansion utilizing realistic casing dimensions indicated densification of the cement and formation of cohesive shear bands as a result of the local expansion (Wolterbeek et al., 2021b). In addition to retaining the integrity of the casing, perceived benefits of this remediation technology include wireline deployment, allowing for a relatively small footprint operation, and less risk compared to cutting and pulling or milling.

The effectiveness of LCE technology in reducing the permeability of leaking annuli has been proven both in extensive laboratory tests (Wolterbeek et al., 2021b), and as part of field trials using the e-line deployable tool. To date, over 50 wells have been successfully treated using localized casing expansion (LCE) technologies. For specific examples of field applications, see the studies of Wolterbeek et al. (2021b) and Green et al. (2021). We build on the current experience with LCE technology and report remediation experiments involving full-scale cemented annulus test assemblies with well-defined, larger-scale migration paths on top of the annular cement. The defects were most likely linked to free water separation from the cement slurry during curing, which occurred unintentionally as part of a full-scale cementing experiment. A conventional cement slurry with additives was used in the construction of the assemblies and the slurry was mixed using a field scale batch mixer. As such, the assemblies studied in this work are considered representative for inclined sections of wells where free water problems may develop during curing. We used a 7 in. model Local Expander tool (Cornelissen, 2019) to perform the inner casing expansions and conducted pressure tests to study permeability reduction. Subsequently, the assemblies were sectioned for visual inspection of the remediated annuli. Access to the affected cement and casing also enabled mechanical characterization using Vickers hardness testing, which is a material characterization technique based on measuring the plastic deformation generated by a standard indenter (Oliver and Pharr, 1992; Liu et al., 2020; Zhang et al., 2018). This technique has previously been performed at the nano- and micro-scale to assess development of cement phases during hydration (Wang et al., 2019; Pedrosa et al., 2020; Constantinides and Ulm, 2004) and for evaluating cement alterations caused by exposure to different fluids (Frech-Baronet et al., 2017; Anwar et al., 2021).

The outline of the paper is as follows. In Section 2 we present the construction of the test assemblies in some detail and go on to characterize the well-defined defects in Section 3. The plan for the remediation experiment is presented in Section 4 and we present permeability measurements based on flow tests with water and with gas in Section 5. Further, in Section 6 we discuss visual observations and hardness testing of annular cement after the assemblies were cut and opened. Finally, we present our conclusions in Section 7.

2. Remediation experiment test assemblies

As part of a full-scale fluid displacement and cementing experiment previously presented by Skadsem et al. (2019), four annulus test assemblies were constructed and finally cemented at near-horizontal inclination in November 2017. After allowing the cement to cure, the test assemblies were found to contain free water channels along the top of the cement, a well-known defect that can compromise zonal isolation over long distances (Nelson and Guillot, 2006; Webster and Eikerts,

Fig. 1. View of the four test assemblies draped in insulation and plastic covers.

1979; Sabins, 1990). Due to their relevant and relatively well-defined defect, two test assemblies were subsequently selected for the LCE remediation experiments described in the current study. For completeness, we will discuss the test assembly configuration and cementing operation below, in addition to initial characterization of the annular cement prior to remediation efforts. Some additional details about the cementing operation can be found in Skadsem et al. (2019), but all pertinent details will be provided below.

A central motivation for constructing the four test assemblies in the first place was to study cement placement in a narrow and near-horizontal annulus, and to detect possible effects of a sudden hole enlargement on the cement quality within and above the enlargement. The four test assemblies were each constructed of two joints of 7 in. casing (32 lbm/ft, 13CR80) placed inside 9 5/8 in. casing (53.5 lbm/ft, P110). A series of test ports were drilled through the top and bottom walls of the outer 9 5/8 in. casing to allow monitoring of the displacement process, and to perform pressure testing of the cemented annuli after the cement had hardened. No attempts were made to centralize the inner tubing in these assemblies, so in most cases the tubing rested on the low side of the casing, supported by its collar on the bottom wall of the annulus. Before cementing, the assemblies were inclined to 85° from the vertical, resulting in near-horizontal cementing conditions. The assemblies were wrapped in wool insulation to provide protection from ambient temperature variations and to stabilize elevated curing temperature by retaining some of the heat generated during curing. A view of the near-horizontal test sections is provided in Fig. 1. The assemblies were here draped in white plastic to cover the insulation wrapped outside the 9 5/8 in. casing sections.

Cementing of the assemblies was performed sequentially. First, a 1.4 s.g. water-based spacer fluid, weighted using baryte and viscosified using a polymeric additive, was circulated through the assemblies. Subsequently, a conventional Class G cement slurry with standard additives such as retarder, defoamer and stabilizer (see Table 1) was mixed and injected to displace the spacer fluid. A KCl brine was used for the slurry mixing water, in order to allow monitoring of spacer fluid displacement and cement placement using conductivity probes mounted at designated positions along the test sections. The cement slurry was mixed at the site of the cementing experiments using a standard offshore type batch mixer with two mixing compartments, each with capacity of 8 m^3 fluid.

Fluid injection into the assemblies was down the inner casing. A wiper ball was initially mounted at the upper end of the 7 in. casing to ensure physical separation of the spacer fluid and the cement slurry during injection down the assemblies. The wiper ball was captured at the bottom of the 9 5/8 in. casing, allowing cement slurry to flow back up toward the upper end of the assembly in the annular space outside the 7 in. casing.

Table 1
Cement slurry composition.

Ingredient	Quantity
Class G cement	100% BWOC
KCl brine (3% BWOS)	37.28 l/100 kg
Fluid loss additives	4.5 l/100 kg
Free water control additive	3.5 l/100 kg
Retarder	1 l/100 kg
Defoamer	0.1 l/100 kg

Once a predetermined excess volume of cement slurry had been injected, pumping was discontinued and the injected cement slurry was pressurized to 5–8 bar by connecting the water main to the upper end of the assemblies. At this point, the assemblies were filled with the curing cement slurry both inside the inner casing and in the annulus between the casings. The assemblies were allowed to cure for 7 days before a first pressure test of the annulus cement was performed. Subsequent pressure and flow testing was performed several weeks later, followed by sectioning of the assemblies into shorter segments that have been stored at the yard for almost 3 years prior to performing the remediation experiments reported herein.

3. Characterization of test assemblies selected for treatment experiments

As part of the pressure and flow testing of the four assemblies mentioned above, it became evident that continuous fluid migration channels existed at the top of the annulus cement. While pressure testing alternately through the test ports mounted along the top side of the assemblies and along the bottom side, it was concluded that the channels were located along the top side of the annulus and spanning most of the length of the test sections. At the time, the existence of the channel was attributed to either incomplete spacer fluid displacement or free water separation from the cement, promoted by the severe inclination of the test assemblies (Nelson and Guillot, 2006; Webster and Eikerts, 1979). Following the initial pressure and flow testing, the four test assemblies were sectioned into shorter segments for visual inspection of the cement quality across the cut surfaces. Based on these preliminary findings, two test assemblies were selected for treatment experiments using LCE technology. We label the sections A2 and C6 in the following and provide photographs of the exposed ends of these assemblies in Fig. 1. Assemblies A2 and C6 were 8.8 m long and 8.3 m long, respectively, and originated from two different, original full-length assemblies. Assembly A2 had a relatively smoothly varying channel at the top of the annular cement while assembly C6 had a similar channel at its far end (8.3 m), but particularly poor cement at its near end (0.0 m). We note the existence of a migration channel also along the top of the cement within the inner casing. This was particularly evident in assembly C6 but the channel was also present in A2. Since a wiper plug was used inside the inner casing for the purpose of eliminating slurry contamination during injection down the test assemblies, we believe that the observed migration channels can be attributed to free water during curing and not slurry contamination (Skadsem et al., 2019). For further characterization of the annular channels, the cement inside the inner casing was removed by water jetting, leaving the two casings and the annular cement sheath.

The annular migration paths were characterized by (1) flow testing and (2) physical point measurements using a measurement stick inserted through test ports drilled in the outer casing. Based on the physical point measurements, the maximum gap width was estimated to be between 1 and 1.5 mm in assembly A2 and between 1 and 15 mm in assembly C6. These measurements agreed with visual inspection of the exposed end cross sections (Fig. 2). The largest gap width in assembly C6 was measured through a test port close to the near end at 0.3 m.

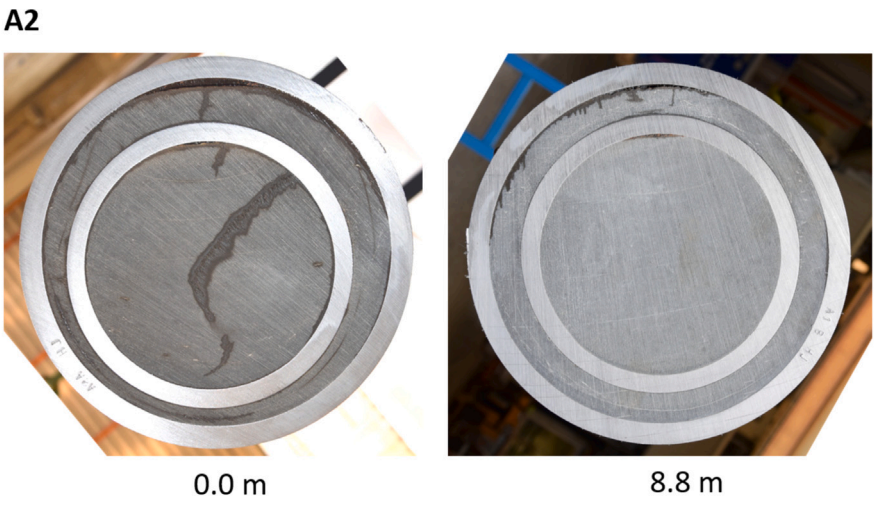

(a) In assembly A2, the eccentricity of the inner 7-in. tubing is approximately 0.45 at the left end (0.0 m) and close to centralized at the right end (8.8 m). Continuous millimeter-sized channels were present on the top side of the cement in the annulus and in the tubing.

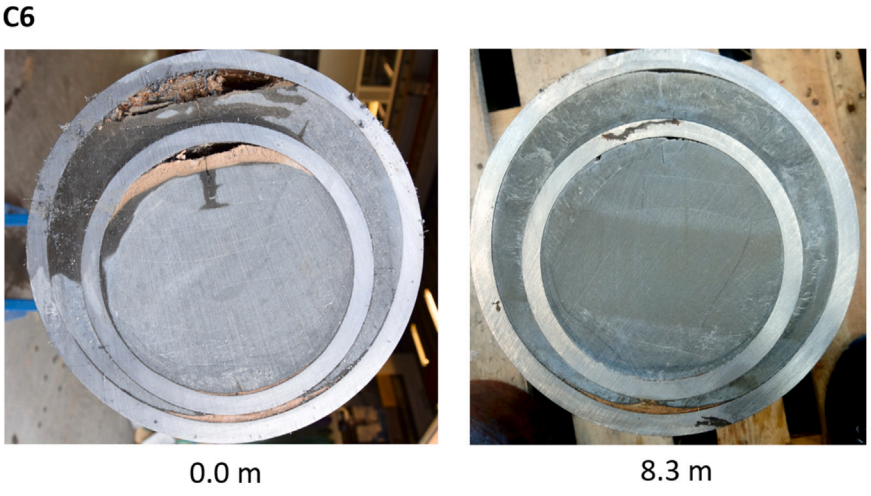

(b) In assembly C6, the eccentricity of the inner 7-in. tubing is approximately 0.75 at the left end (0.0 m) and approximately 0.6 at the right end (8.3 m). Debris, voids and severely fractured cement occupied the annular space at the left end of the test assembly. The condition of the annulus cement improved toward the right end where a millimeter-sized channel remained.

Fig. 2. Ends cross sections of test assembles A2 and C6 selected for the remediation experiment.

Subsequently, flow tests were performed to confirm the physical measurement described above and to connect the channel size to an effective annulus permeability. To this end, a pump was used to apply a constant water pressure, $\Delta\hat{P}$, to a test port at one end of the assembly. At the other end we measured the volumetric flow rate, $\hat{Q}$, produced through an open test port a distance, $\Delta\hat{L}$, away from the inlet. The measurements were used in conjunction with the Darcy equation

$$\hat{Q} = \frac{\hat{k}\hat{A}}{\hat{\mu}} \frac{\Delta\hat{P}}{\Delta\hat{L}}. \tag{1}$$

to estimate the effective permeability, $\hat{k}$. Here, $\hat{A}$ is taken to be the cross-sectional area of the annulus between the 7 in. inner casing and the inner wall of the outer 9 5/8 in. casing, and $\hat{\mu}$ is the viscosity of water, assumed 1 mPa·s in calculations. For the inner diameter of the 9 5/8 in. casing, we take a nominal value of 0.2168 m. The flow measurements presented in Table 2 confirm that C6 has the largest free water channel, and indicate initial permeabilities ranging from approximately 80 up to hundreds of darcy.

To connect the effective permeability estimates to an effective channel gap width, we consider the idealized geometry shown in Fig. 3. Here, the channel is bounded above by a circular arc of radius $\hat{a}$ within the angular interval $[-\theta^*, \theta^*]$, with $\theta^* = \arccos(1 - \hat{h}/\hat{a})$, and below by the horizontal line at a radial distance $\hat{\alpha}(\theta)$ from the center

Table 2
Flow testing of test assemblies prior to treatment.

Assembly	$\Delta\hat{P}$	$\Delta\hat{L}$	$\hat{Q}$	$\hat{k}$
A2	5.9 bar	8.2 m	3960 ml/min	77 darcy
	5.8 bar	8.2 m	4080 ml/min	80 darcy
C6	1.4 bar	6 m	4080 ml/min	243 darcy
	1.3 bar	6 m	5580 ml/min	364 darcy

of the circular arc. The circular arc corresponds to the inner wall of the 9 5/8 in. casing, while the horizontal line is the top of the annular cement. By assuming fully developed, laminar flow, we use the hydraulic diameter (White, 1991) of the geometry in Fig. 3 to approximate the volumetric flux as

$$\hat{Q} = \frac{T(h)\hat{a}^4}{\hat{\mu}} \left(-\frac{\partial\hat{p}}{\partial\hat{z}} \right), \tag{2}$$

where

$$T(h) = \frac{\left(\theta^* - (1-h)^2 \tan\theta^*\right)^3}{8\left(\theta^* + \sin\theta^*\right)^2}, \tag{3}$$

and $h = \hat{h}/\hat{a}$. The constant friction pressure gradient is denoted by $-\partial\hat{p}/\partial\hat{z}$. We identify the function $T(h)$ as a dimensionless transmissivity

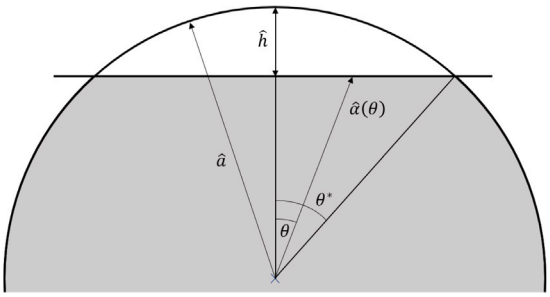

Fig. 3. Geometric model to represent flow in a uniform free-water channel.

function and plot $T(h)$ as the solid line in Fig. 4. To confirm the validity of the hydraulic diameter approach, numerical solutions of the exact momentum conservation equation

$$\frac{1}{\hat{\mu}}\frac{\partial \hat{p}}{\partial \hat{z}} = \frac{\partial^2 \hat{u}}{\partial \hat{r}^2} + \frac{1}{\hat{r}}\frac{\partial \hat{u}}{\partial \hat{r}} + \frac{1}{\hat{r}^2}\frac{\partial^2 \hat{u}}{\partial \theta^2}. \tag{4}$$

are included as points in Fig. 4. Here, $\hat{u}$ denotes the axial velocity of the fluid. As expected, the two approaches are in excellent agreement (White, 1991).

Turning to the two test assemblies A2 and C6 and the measurements in Table 2, we equate $T = \hat{k}\hat{A}/\hat{a}^4$ and find an average $T \approx 6.8 \cdot 10^{-9}$ for assembly A2 and $T \approx 2.6 \cdot 10^{-8}$ for assembly C6. As indicated in Fig. 4, these values of the transmissivity function correspond to $h \approx 0.009$ for A2 and $h \approx 0.013$ for C6. Converting to physical units, we estimate a maximum gap width of 1 mm for assembly A2 and 1.4 mm for C6. These estimates agree well with the physical gap width measurements and suggest that indeed the seepage potential prior to treatment was largely determined by channel widths of 1 to 1.5 millimeters in either assembly.

Finally, to confirm that flow is dominantly occurring through the channel at the top of the annulus, flow testing by injecting either cold or warm water and imaging the external surface of the assemblies using infrared thermography (IRT) was performed. The test was performed by first injecting warm water maintained at approximately 40 °C while monitoring the surface temperature of the outer casing using IRT. The warm liquid quickly heated the adjacent casing and the resulting surface temperature profile provided another indication that flow was primarily through the distinct gap at the top of the annular cement. Subsequent injection of cold water had the reverse effect of locally cooling the casing, initially along the migration channel. Fig. 5 presents three photographs for the experiment performed with assembly C6. Fluid flow was here from right to left and a thin piece of metallic tape was placed at 1 m intervals to enable axial tracking of the temperature profile. The assemblies were rotated about their axis as part of the test to prove that flow was only through the identified top annular channel.

For assembly C6, some uneven heating spots in the interval from 0.0 to 3 m were observed. These are indicated in Fig. 6 and are likely connected to the poor initial cement quality in this end of assembly C6. Fig. 6(b) shows a side view of part of the assembly, showing that the surface heating of the outer casing occurred at the orientation of the top annular channel.

4. Remediation by local expansion of inner casing

Once the initial characterization of the cemented assemblies was complete, the assemblies were selected for a remediation experiment involving local mechanical expansion of the inner casing. The prior removal of the inner casing cement by water jetting allowed running the 7 in. model of the Local Expander tool (Cornelissen, 2019) inside the assemblies. Specifications of the tool used in the experiments are presented in Table 3 and a comprehensive account of the Local Expander tool technology and field experience is provided by Wolterbeek et al. (2021b).

Table 3
Specifications of Local Expander tool used in the remediation experiments.

7 in tool specifications	
Expandable head — OD (collapsed)	153 mm
Expandable head — OD (expanded)	174.4 mm
Body tool — OD	143 mm
Max. radial increase	12 mm
Max. stroke length	140 mm
Max. axial force	1438 kN
Tool length	4 m
Tool weight	350 kg

Table 4
Position and order of dents. Reference is made to Fig. 8 for a visualization of the dents relative to test ports and the ends of the assemblies.

	Current	Dent order						
Set name	(A)	1	2	3	4	5	6	7
A2-1	3.95	2.4	1.8	2.1	–	–	–	–
A2-2	4.26	4.2	4.8	4.5	–	–	–	–
A2-3	4.27	6.0	6.5	6.4	6.3	6.2	6.1	–
A2-4	4.27	7.7	–	–	–	–	–	–
C6-1	4.46	1.6	1.0	1.3	–	–	–	–
C6-2	4.47	4.0	4.9	4.8	4.6	4.5	4.3	4.2
C6-3	4.47	7.2	–	–	–	–	–	–

The tool contains an active expandable head which consists of sixteen hardened steel fingers visible in Fig. 7.

It can be run freely in the well while in its unexpanded configuration where the fingers are collapsed onto the tool axis. Once activated, an actuated cone inside the tool drives the fingers radially outward and results in local plastic deformation of the inner casing and compression of the confined annular cement. As discussed in the introduction, when well cement is effectively confined, it can accommodate significant strain levels before losing its load-carrying capacity and overall mechanical integrity. An impetus for the current remediation experiment is to study if the inner casing expansion and cement compression can treat millimeter-sized and relatively large free water channel at the interface to the *outer casing*.

The remediation experiment was performed in an indoor test hall and using a dual winch system to correctly position the tool inside the test assemblies. Several sets of dents were planned at different positions in the two assemblies and additional pressure ports were mounted to allow flow testing of individual sets of dents. The test ports were installed at the top of the annulus, ensuring direct communication with the migration channel at the top of the annular cement. The axial positions of the planned dents are shown in Table 4 where the lengths are measured in accordance with the cross-sectional orientations in Fig. 2 and the schematic provided in Fig. 8. As indicated, combinations of single and multiple dents were planned in order to gauge possible further reductions in annulus permeability with subsequent dents placed adjacent to each other. The order of dents is also indicated in Table 4. At locations where multiple dents were planned, the order of the dents was generally such that the left-most and right-most dents were placed first followed by the central dents. Also listed in Table 4 is the maximum tool current configuration in each of the sets of dents. The maximum current is indicative of the degree of pressure exerted on the inner casing wall by the tool, with the higher maximum current resulting in greater maximum pressure applied on the wall.

Before placing the first dent in any one set, communication was confirmed between the test ports at either side of the planned set of dents. As indicated by the direction of flow testing in Fig. 8, this was achieved by connecting a pump to the test port immediately to the left of the current set of dents. The test port immediately to the right was kept open to the atmosphere. Water pressure was applied at the inlet port and the resulting flow rate was measured by a Coriolis flow meter mounted between the pump and the inlet port. The measuring range

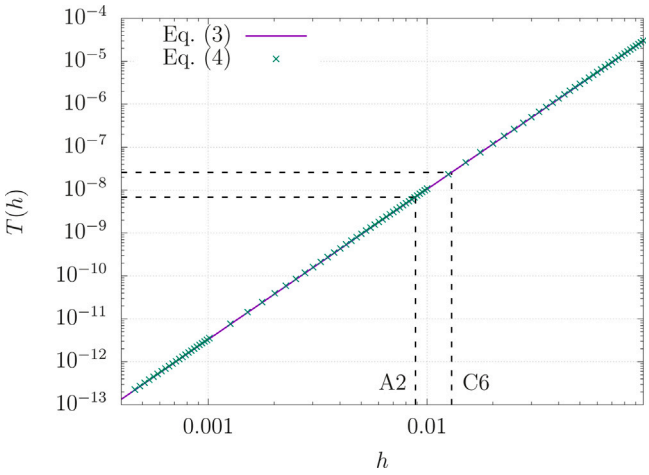

Fig. 4. Evaluation of the transmissivity function Eq. (3) (solid line) for fully developed, laminar flow along a channel of circular section shape, Fig. 3. Shown as points are numerical solutions to the exact axial momentum conservation equation.

(a) Test section C6 with metallic tape for position identification.

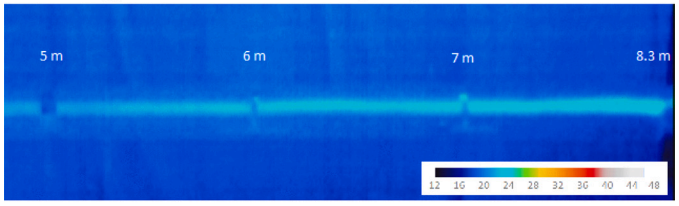

(b) Initial stage of warm water (40°C) injection. The flow is from right to left and the infrared thermography picture was taken 3 minutes after start of injection.

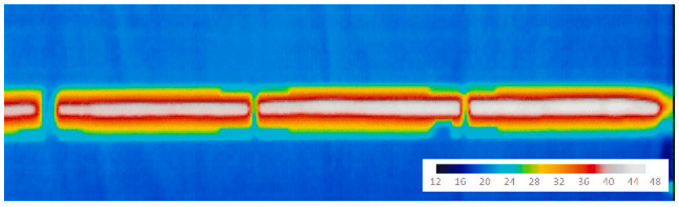

(c) Final stage of warm water (40°C) injection. The flow is from right to left and the infrared thermography picture was taken 30 minutes after start of injection.

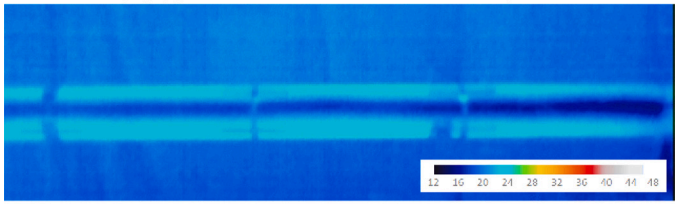

(d) Final stage of cold water (10°C) injection. The flow is from right to left and the infrared thermography picture was taken 10 minutes after start of cold water injection.

Fig. 5. Sequence of images using infrared thermography during base line flooding test in section C6. The photographs are from the interval between 4.8–8.3 m, at the right end of the assembly. Temperatures are in units of degree Celsius.

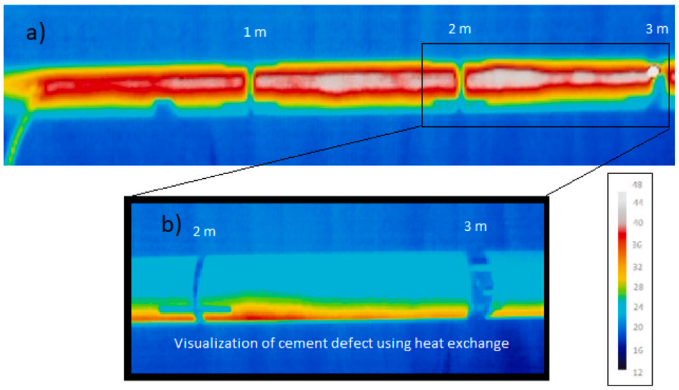

Fig. 6. Warm water (40 °C) injection in assembly C6. Water is injected from right to left. (a) Picture of the interval between 0.0 m and 3 m after 30 min since start of injection. (b) Detail of a part of the assembly rotated by 90° showing that surface heating was limited to the region of the migration channel.

for the Coriolis flow meter was up to 85.9 ml/min. The measured flow rate before denting was in all cases higher than the range of this sensor for even the smallest applied pressures, confirming no measurable resistance to flow in agreement with the initial assembly characterization. Once pressure and flow communication were confirmed, pumping ceased and the tool placed the first dent in the current set. After denting, another flow test was performed to evaluate the new, effective annulus permeability. Subsequent dents within the same set were then placed, with new flow tests performed after each successive dent. In all cases, water was used as the working fluid for flow testing during the remediation experiment between successive dents. In addition to this, longer-term pressure testing with gas as working fluid was performed post-remediation. In the following section, we present results of both types of flow and pressure testing and continue in the subsequent section by presenting visual inspection of dented intervals and Vickers hardness test of original and of deformed cement.

5. Remediative permeability reduction

5.1. Flow testing with water

To assess the effective annulus permeability following successive dents, measurements of volumetric flow rate, $\hat{Q}$, at a specified differential pressure, $\Delta\hat{P}$, are used in conjunction with the Darcy equation (1).

Fig. 7. The casing expansion tool partly inside one of the test assemblies. A dual winch system was used to position the tool inside the assemblies prior to each dent.

As before, $\hat{A}$ is taken to be the cross-sectional area of the annulus between the 7 in. inner casing and the outer 9 5/8 in. casing. Since the flow restriction between test ports is now mainly due to the dents, we assume that the pressure drop between the inlet and outlet ports occurs locally at the dents, *i.e.* over a short length of *treated* annular cement, $\Delta\hat{L}_{set}$. Based on post-treatment photographs of the cut test assemblies to be presented in the following sections, we consider each dent to affect the cement over an interval of approximately 8 cm. That is, we take $\Delta\hat{L}_{set} \approx 0.08N$ m with N being the total number of dents placed between the test ports used for flow testing. The effective permeability per set of dents can now be assessed and we summarize the results in Fig. 9, where we also indicate the initial permeabilities from Table 2. The permeabilities indicated in the figure are based on flow measurements after setting all individual dents in each set, and are given in units of millidarcy (mD), or $9.87 \cdot 10^{-16}$ m^2. Also shown in the figure and indicated by an asterisk to the set of dents, are results of seepage testing with gas. These are discussed in more detail in the next subsection.

In most cases of water flow testing, the pressure provided by the test pump was increased in steps up to approximately 100 bar pressure. This significant pressure differential applied over a very short section represents severe and relatively extreme conditions compared to anticipated downhole conditions, resulting in major elastic deformation of casings and adverse test conditions. Additionally, the measurement durations were relatively short (on the order of few hours per set). Consequently, some of the measured flow may be related to specific storage effects (*e.g.*, pressurization of the cement pore space). The reported permeability values should therefore be considered upper estimates. To estimate the magnitude of the elastic casing deformation, we may use the thin-wall cylinder expression $\hat{u}_r = \hat{P}\hat{R}^2(1-\nu/2)/(\hat{E}\hat{t})$, where $\hat{u}_r$ denotes the radial displacement of the casing wall, $\hat{P}$ is the pressure difference between the inside and outside of the casing, $\hat{R}$ is the mean radius of the casing, $\hat{E}$ and ν are the Young's modulus and Poisson ratio of the casing and $\hat{t}$ its wall thickness (Roylance, 1996). Setting $\hat{E} = 210$ GPa and $\nu = 0.3$ for the casing steel, and assuming nominal wall thickness of 0.0138 m for the 9 5/8 in. casing, we find a radial expansion of 38.9 μm with 100 bar internal casing pressure. From the Darcy flow equation, we may convert a uniform microannulus of width $\hat{h}$ to an effective permeability $\hat{k}$ using $\hat{k}\hat{A} \leftrightarrow \hat{W}\hat{h}^3/12$, with $\hat{A}$ the annular cross-sectional area between the 7 in. and 9 5/8 in. casings and $\hat{W}$ the inner wall circumference of the 9 5/8 in. casing. Using nominal values for the casing dimensions, we find that a uniform microannulus of width 38.9 μm at the interface between the annular cement and the inner wall of the 9 5/8 in. casing is equivalent to an effective annulus permeability of approximately $2.8 \cdot 10^{-13}$ m^2 or 0.28 darcy. This is significantly higher than the effective permeabilities for the successful dents in Fig. 9 and further evidence of highly effective sealing. We recall from Table 2 and Fig. 4 that the initial effective permeability was estimated to be in the range of approximately 80 to hundreds of darcy. Even at such extreme test pressures considered here, the effective permeability was less than 0.1 mD for all but two sets of dents, indicating the effectiveness of the technology in reducing the permeability several orders of magnitude.

In sets A2-2, A2-3, A2-4, C6-2 and C6-3, made up of either one, three, six or seven dents, the effective permeability in all cases decreased to a level below 0.1 mD after the dents had been set. The majority of the permeability reductions occurred once the first dent was set. In some cases, a slight further reduction was observed, but generally the first dent reduced the permeability to below 1 mD in these sets. We also observed that even a single dent, such as C6-3, gave a permeability reduction comparable or even larger than that of multiple dents, *e.g.* sets A2-3 or C6-2. The two sets of dents A2-1 and C6-1 did not result in an effective permeability below 10 mD. The first set, A2-1, consisted of three dents and resulted in 30 mD permeability after the first dent and no further reduction from the subsequent two dents. We note that this was the initial set of dents that was performed in the remediation experiment and we attribute the higher permeability to the tool configuration being set to a low expansion level. In subsequent sets, starting with A2-2, the tool current setting was configured to produce more casing expansion and this greatly reduced the permeability in all sets of dents except C6-1, as seen in Fig. 9. Finally, set C6-1, which was placed in the poorly cemented side of assembly C6, resulted in an effective permeability of the order of 1 darcy following the three dents. The result was not unexpected considering the relatively fragmented and highly flawed cement that was believed to occupy this part of assembly C6 (see Fig. 2(b)). In this case, the configured tool expansion level combined with the initial poor cement quality probably resulted in inadequate cement compression. Still, the expansion resulted in what appears to be at least a hundredfold decrease in permeability, suggesting that the annular cement was providing substantially more resistance to flow compared to the pre-remediation state. To summarize, dents were set in assemblies A2 and C6 at different degrees of expansion (less in A2-1 than in the other sets) and in positions along the assemblies with variable initial cement quality (the cement at set C6-1 being worse than at the other sets). The observed permeability reductions suggests that the final permeability post-remediation is linked to both parameters and, as long as sufficient cement confinement can be achieved, that increased casing expansion will lead to reduced permeability.

5.2. Gas migration testing

We recall that the flow tests performed during the casing expansion and treatment of the test assemblies were performed at high differential pressures for the low-permeable sets of dents. As much as 100 bar pressure was applied over a few meters length between the test ports, representing far harsher conditions than those expected downhole. To probe the permeability of some dents at lower differential pressures, a second test campaign involving gas migration testing was performed post-remediation of the assemblies. This second campaign consisted of connecting pressurized N_2 gas to one injection port and measuring pressure build-up or flow through adjacent ports opposite sets of dents. In test assembly A2, 25 bar of N_2 was first connected to the test port at 5.2 m, as defined in Fig. 8. Pressure sensors connected to the ports at 3.1 m (*i.e.*, covering A2-2) and 7.4 m (*i.e.*, covering A2-3) registered no pressure build-up over a test period of 7 days. The permeability of these dents are therefore considered below the detection limit ("BD") of

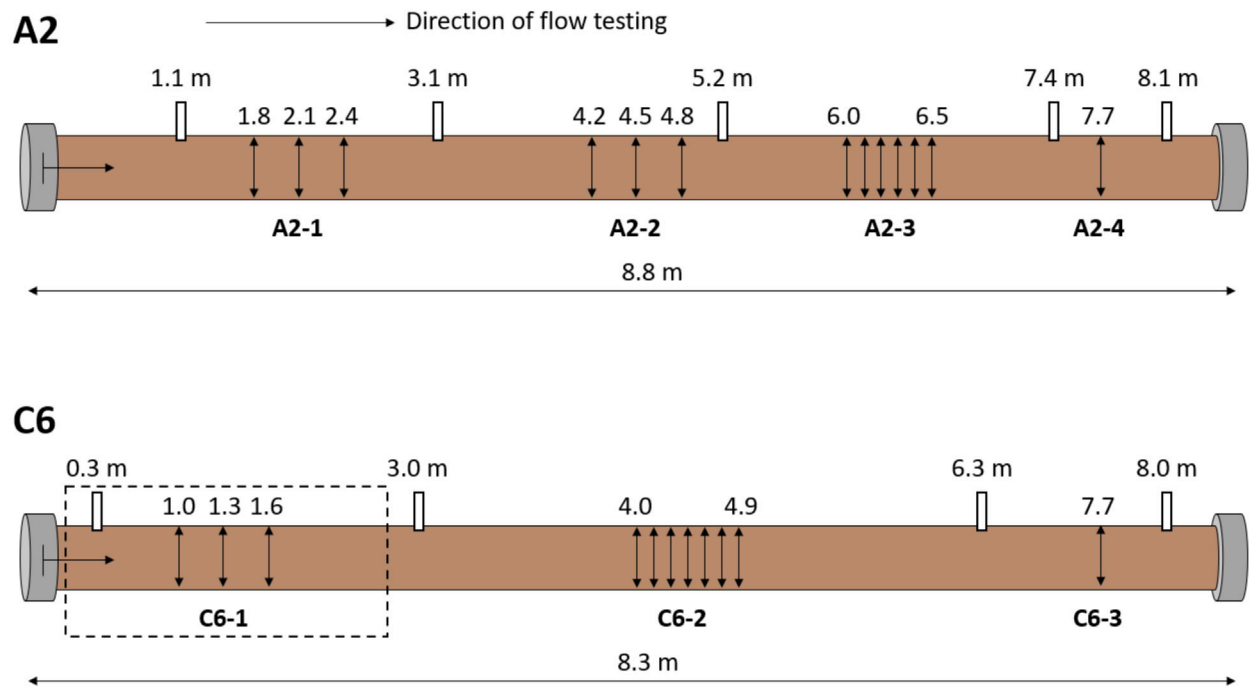

Fig. 8. Configuration of dents and pressure and flow test ports in the two test assemblies. The annular cement at set C6-1 was known to be in very poor initial condition and this segment is indicated by the dashed rectangular box. Assembly A2 and the remainder of C6 had continuous millimeter-sized channels on the top side.

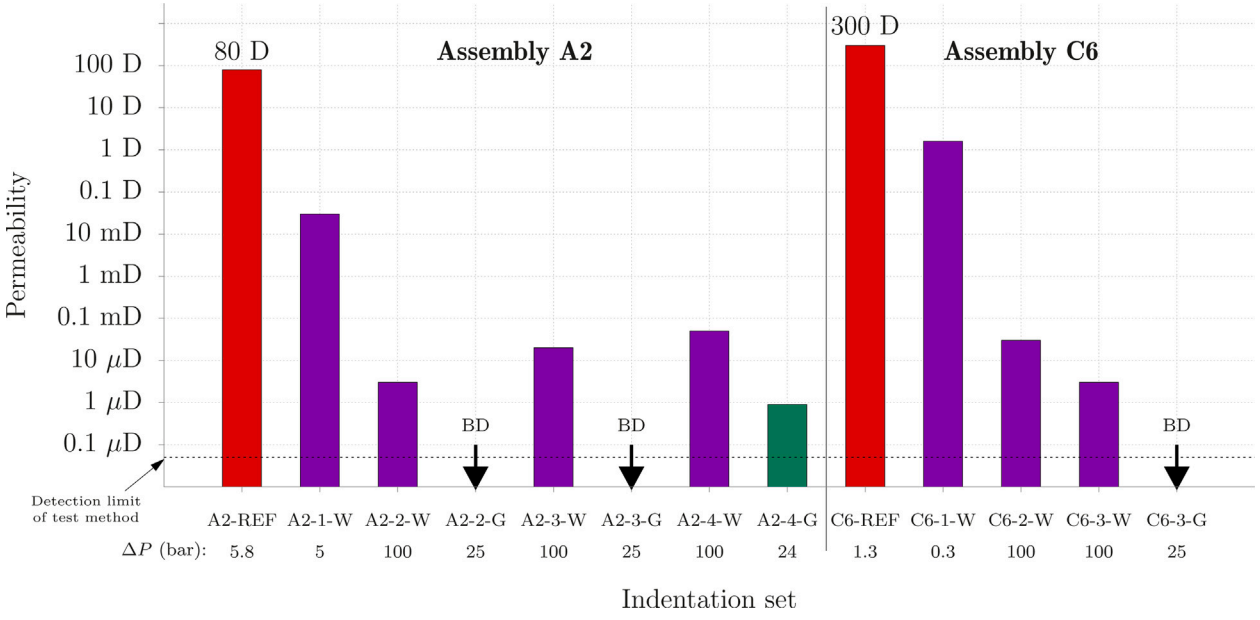

Fig. 9. Permeability measurements following the final dent per set of dents. The labels of the sets of dents are here appended with capital letter "W" or "G" to indicate whether the permeability is based on seepage testing with water ("W") or with gas ("G"), respectively. The differential pressure used when determining the permeability is listed in parenthesis, below the label. For dents (sets) A2-2-G, A2-3-G and C6-3-G, the measured gas flow rate or pressure buildup was too low and no measurable permeability could be quantified (indicated using "BD" = "below detection", at an estimated permeability of 0.05 μD). For reference, the average initial permeability prior to treatment, as per Table 2, is indicated by the bars labeled A2-REF and C6-REF.

0.05 μD in Fig. 9. The defined detection limit is based on a conservative assessment of the volumetric gas flux that is required to increase the annular pressure between dents by 1 bar over approximately 1 h. In practice, the actual detection limit was likely lower than this value.

Moving the N_2 injection point to the port at 7.4 m, pressure was detected at the port at 8.1 m. A flow test at 24 bar pressure yielded a gas seepage rate of 13 ml/min across the single dent A2-4, corresponding to an annular permeability of approximately 0.9 μD, which is comparable to that of intact bulk cement (Nelson and Guillot, 2006). In test assembly C6, N_2 pressure was supplied to the port at 6.3 m. While maintaining a constant pressure of 25 bar N_2 pressure over a period of 24 h and having a bubble catcher connected to the port at 8.0 m (*i.e.*, covering C6-3), we recorded merely 5–7 ml of N_2 to escape from the port. This suggests C6-3 had an even lower gas permeability than that measured in assembly A2 (estimated well below 0.05 μD). These

Fig. 10. Illustration of axial cut (top) and cross-sectional cuts (bottom) for assessing remediated annular cement.

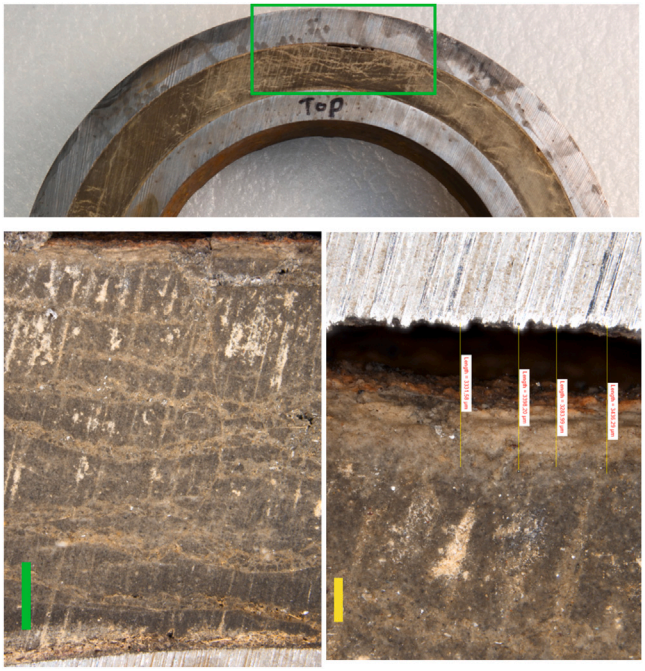

Fig. 11. Close-up view of the cement next to the migration channel at position 2.15 m in test assembly A2. The radial distance between the top of the annular cement and the inner wall of the 9 5/8 in. casing is measured to approximately 3.3 mm. The green color bar in the left bottom photograph is 5 mm long while the yellow bar in the right bottom photograph is 1 mm long. (For interpretation of the references to color in this figure legend, the reader is referred to the web version of this article.)

Fig. 12. Results of Vickers hardness testing in the region shown in Fig. 11.

test results suggest that the initial gas permeability through the water-saturated and treated assemblies are close to that of intact bulk cement. Due to the extremely low seepage rates, no further attempts were made to estimate the effective permeability post-treatment.

Similar permeability reductions as those reported here have also been found in the study of Kupresan et al. (2014) where a driven expansion cone was used to expand the inner casing, and in previous controlled laboratory testing of the Local Expander tool (Wolterbeek et al., 2021b). Our findings support these observations and suggest certain effectiveness also when the initial cement condition is poor, as evidenced by set C6-1.

6. Characterization of annular cement following treatment

Following the seepage testing discussed above, the treated assemblies were next opened for visual inspection of the annular cement at the positions of the dents and in the immediate proximity of the remediated regions. In addition to direct visual inspection, several cuts were also subjected to Vickers hardness testing to identify possible mechanical alterations of the cement following denting and plastic deformation (Smith and Sandly, 1922; Igarashi et al., 1996; Anwar et al., 2021). Vickers hardness testing was performed by first polishing the cuts using 18 μm (P1000) and then 10 μm (P2000) SiC paper followed by rinsing with water and ethanol for a relatively smooth surface. The hardness was measured using a diamond pyramid indenter pressed into the cement with a load of 0.5 kg mass force and 10 s dwell time. As the cement close to the top annular channel was relatively heterogeneous, the load was fixed to the value of 0.5 kg mass force to allow the pyramid indentations to cover a sufficiently large area and give representative measurements of hardness. The hardness measurements shown below are in standard hardness testing units of mass force by area in units of mm^2, or HV. Hardness testing of a previously retrieved cement core from the inner casing cement (retrieved prior to removal of the casing cement) gave an average hardness value of 33.7 HV for this batch of cement with a standard deviation of 2.5 HV. The hardness of the casing wall itself was measured using 3 kg mass force, and was found to be 305 HV with a standard deviation of 5 HV when tested away from the position of the dents.

Mainly the two types of cuts illustrated in Fig. 10 were performed, namely (1) axial cuts intended to expose annular cement variations at different distances from the dents along the top and bottom side of the annulus, and (2) about 5 cm thick cross-sectional cuts. In the latter cuts, one face exposed the annular cross-section directly at the dent location, while the other face gave the cross-section 5 cm away from the dent. Due to the residual stress accumulated in the casing steel, care

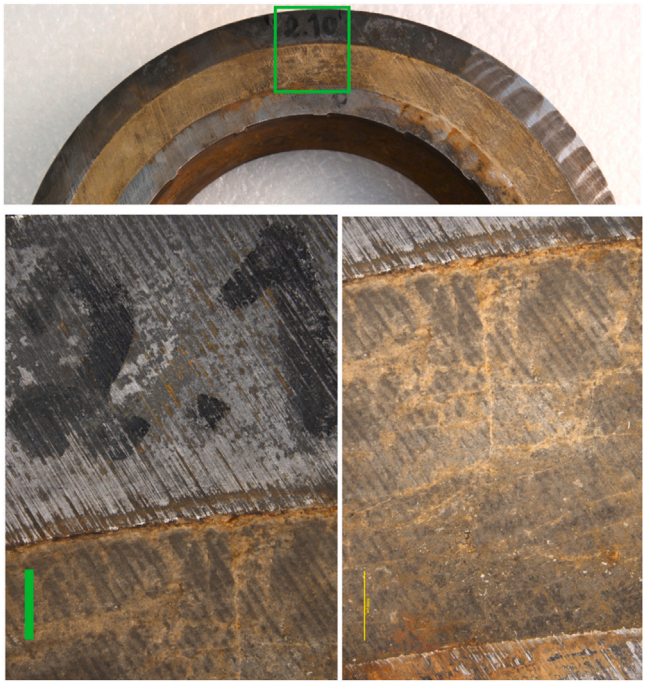

Fig. 13. Close-up view of the cement next to the migration channel at dent position 2.1 m in test assembly A2. The green bar in the left bottom photograph is 5 mm long. This scale applies to both photographs in the bottom panel of the figure. (For interpretation of the references to color in this figure legend, the reader is referred to the web version of this article.)

needed to be taken to make the cuts without jamming the saw blade or disrupting the contact between cement and casing.

In Fig. 11 we provide a detailed view of the cement in the proximity of the channel from a cross-sectional cut at position of 2.15 m from the left end of assembly A2. This position is 5 cm to the right of the dent at 2.1 m. As can be seen from the photographs in the bottom panel of Fig. 11, the cement is relatively heterogeneous in this top part of the annulus, exhibiting what appears to be a layered structure with horizontal bands. The bottom right photograph suggests a gap width of approximately 3.3 mm at this position. Vickers hardness testing results from this cement region are shown in Fig. 12, giving a considerable spread around an average value of 26 HV. These values are generally lower than the 33.7 HV estimate from the inner casing cement core.

Next, focusing on the dent at 2.1 m in assembly A2, i.e. the center dent in set A2-1, we show in Fig. 13 a close-up of the annular cement at the position where the channel was initially, prior to remediation. Closure of the channel is apparent from the close-ups in Fig. 13. We have not identified new flaws in the cement that could be attributed to the remediation operation. We recall that the effective annulus permeability in this part assembly A2 was approximately 30 mD following the three dents. It is apparent from Fig. 13 that the cement was indeed forced to contact the outer casing but the degree of inner casing expansion was probably not sufficient for generating a seal of comparable permeability as subsequent dents in comparable annular cement. Interestingly, when performing Vickers hardness testing for the section in Fig. 13, an average hardness value of 20 HV was found with a considerable standard deviation of 6HV. This is in fact a slight softening compared to the values shown in Fig. 12 at 2.15 m, merely 5 cm away from the dent location. Vickers hardness measured in the bottom sector of the annular cement at 2.1 m and 2.15 m is found to be 30 HV–31 HV in both cases, overlapping with that of the inner casing cement core when accounting for the standard deviations for both.

An axial view of the dents at 1.8 m and at 2.1 m is provided in Fig. 14. Here, one half of the dent at 2.1 m is shown, the other half

Fig. 14. Axial cross section through the dent at 1.8 m (bottom-most dent) and one half of the dent at 2.1 m (top-most dent). We observe the well-defined migration channel between the dents along the top part of the annulus (to the left in the photograph) and clear cement-casing contact areas at the levels of the two dents.

making up the cross-sectional view in Fig. 13. Between the two dents, we identify the channel at the top of the annular cement. At the dents, the annular cement has been compressed and is here pressing onto the inner wall of the outer casing. From the 1.8 m dent, the bottom-most dent in Fig. 14, we observe visually that the annular cement is in contact with the wall of the inner casing over an axial length of approximately 8 cm. We recall this observation being the basis for determining the effective permeability in connection with Fig. 9. Further, the annular cement has a relatively dense population of minor fractures and flaws away from the dent and we do not observe any obvious defects that could be attributed to casing expansion at the locations of the dents. Finally, Vickers hardness measurements of the dent at 1.8 m are indicated in Fig. 15, showing measurements for both cement and casing steel at the dent and short distances away. We observe a tendency for increased hardness in the cement and in the casing steel although these changes are within the standard deviations of the measurements.

Moving on to the single dent at 7.7 m in test assembly A2, we recall from Fig. 9 that the effective water permeability following this single dent was less than 0.1 mD. Compared to the dents at 1.8 m and 2.1 m studied above, the degree of casing expansion was increased and this contributed significantly to reduce the permeability. In Fig. 16 we show close-ups of the top part of the annular cement at axial positions

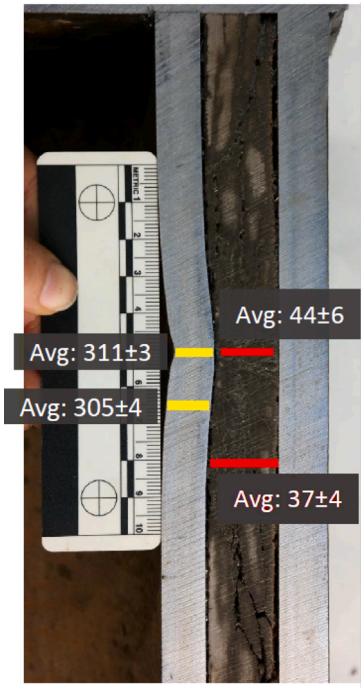

Fig. 15. Dent at 1.8 m presenting measurements of Vickers hardness for cement (red) and steel (yellow). (For interpretation of the references to color in this figure legend, the reader is referred to the web version of this article.)

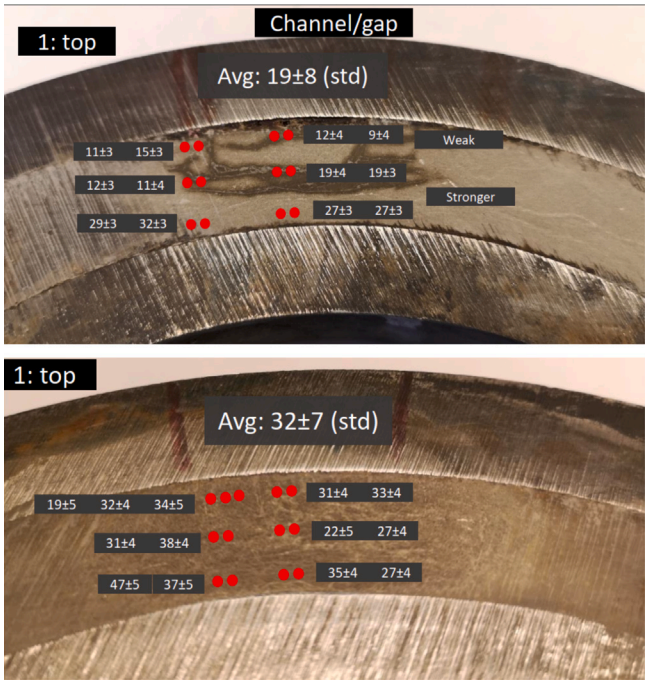

Fig. 16. Cross-sectional cuts at 7.65 m (top, 5 cm to the left of the dent A2-4) and at 7.7 m (bottom, at the dent) overlaid with results from Vickers hardness testing.

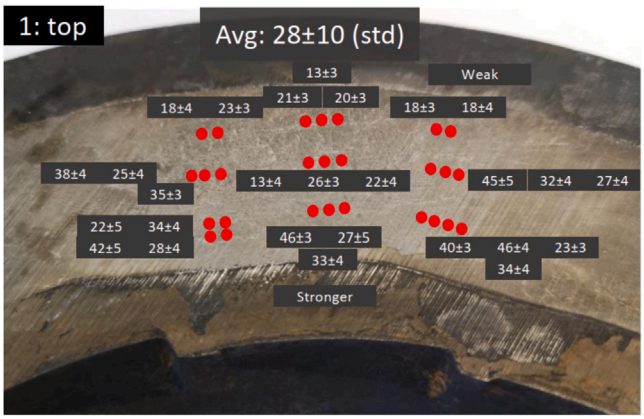

Fig. 17. Results from Vickers hardness testing at the cross-sectional cut in test assembly C6 at axial position 7.2 m. An average value of 28 HV is found, albeit with a considerable spread. The highest hardness values are consistently found close to the wall of the inner casing. We also note the distinct grooves made in the inner casing wall by the hardened steel fingers of the expansion tool.

7.65 m (top panel) which is now 5 cm to the left of the dent at 7.7 m. The bottom panel of the figure corresponds to the top part of the annular cement at the dent position 7.7 m. We again observe the same features as in Figs. 12 and 13, namely a relatively heterogeneous cement next to the migration channel in the top panel of the figure. The Vickers hardness values average to 19 HV with a considerable spread and the lower hardness values found closer to the gap. At the dent, shown in the bottom panel of the figure, we observe again a complete closure of the channel and no obvious, new defects introduced by the casing expansion and cement compression. We also observe a significant increase in Vickers hardness, with an average result of 32 HV and similar to that of the inner casing cement plug. The Vickers hardness of the annular cement in the bottom sector average to 30 HV at both positions shown in Fig. 16. This value is also similar to that found in the bottom sector at 2.1 m and 2.15 m, discussed above.

Vickers hardness measurements have also been performed at the single dent at C6-3, with the results at the position of the dent shown in Fig. 17. We again find a considerable spread in the hardness measurements, with the highest values always being closer to the inner casing. An average value of 28 HV is found with a considerable standard deviation of 10 HV. Hardness measurements acquired at the top annular cement at a position of 7.15 m, a distance of 5 cm to the left of the dent in Fig. 17, indicate an average hardness of 23 HV, with a standard deviation of 5 HV. This is close to, or slightly less than the hardness values at the dent location of 7.2 m.

To sum up the observations related to Vickers hardness testing, we have observed both an apparent softening and a hardening at the locations of the dents. For set A2-1, where inner casing expansion was performed to a lower degree than in the remaining sets of dents, we observed an apparent softening of the cement. This may be due to cement being plastically strained to close the annular gap, but not compressed enough to significantly compact and harden. At dents A2-4 and C6-3, inner casing expansion was greater and this resulted in a lower effective permeability compared to A2-1, as well as a tendency for hardening of the cement close to the gap that was closed by casing expansion. As indicated, these observations may be connected to different levels of cement compression across the three sets of dents studied with Vickers hardness testing. We point out that the standard deviations associated with the hardness values are high and connected to the relatively heterogeneous structure of the annular cement. Future tests involving confined cement compacted to varying degrees before hardness testing will be useful for evaluating this hypothesis further.

Focusing on dents C6-1, set in the poorly cemented part of test assembly C6, the axial view in Fig. 18 reveals the expected very poor and fragmented initial cement condition in this part of assembly C6. However, it is interesting to note what appears to be an improvement in the cement condition at the positions of the two dents in the figure, here indicated by the rectangles, at 1.0 m and 1.3 m from the end of the assembly. Further details can be seen in Fig. 19, where the top panel shows the upper annular cross section at 1.3 m and the bottom panel is

Fig. 18. Axial cross section through the dent at 1.0 m (top-most dent) and one half of the dent at 1.3 m (bottom-most dent). We observe generally fragmented and poor cement away from the dents. At 1.1 m and 1.3 m, the cement appears to have improved cohesion compared to the initial condition seen away from these positions.

Fig. 19. Cross sectional view of the annular cement at the dent placed at 1.3 m in assembly C6 (top panel) and at 1.35 m, or 5 cm to the right of the dent (bottom panel).

from 1.35 m, or 5 cm to the right of the dent at 1.3 m. The dent in the top panel can clearly be made out by the grooves in the inner tubing wall, resulting from the local, mechanical expansion of the tubing. Although both panels show a heterogeneous and flawed cement, the cement at the dent appears to have better cohesion with less fragments compared to the bottom panel which is the cross-section some 5 cm away from the dent. We recall from Fig. 9 that the compressed cement is not sealing the annular space at this level of casing expansion and cement compression, but it is not unlikely that a greater degree of expansion could potentially have reduced the permeability further. It is worth noting here that the forming limit of the pipe was not reached, *i.e.*, in theory much larger radial expansions are possible and could also be imposed using the newest generation of LCE tools.

7. Conclusion

We have studied whether millimeter-sized free-water channels can be remediated using casing expansion generated by a wireline deployable expansion tool. The approach can be used where there initially is sufficient cement to be compressed behind casing, where casing integrity is not compromised as a result of local expansion and where there is sufficient clearance for running the tool. For dents to be set in strongly inclined well sections, a tractor may be required to pull the tool into place. The current study is focused on the treatment of full-scale test assemblies that were cemented using a realistic cement slurry and actual field equipment in November 2017. The resulting migration channels were not a part of the initial design, but likely occurred due to unintentional slurry stability issues. The test assemblies were characterized by a naturally occurring and well-defined migration channel, present at the interface between the annular cement and the inner wall of the outer casing. Initial pressure and seepage tests indicated the location of the channel at the top of the annular cement and subsequent infrared thermography and finally cuts confirmed the channel position. The effective permeability of the continuous migration channels was estimated to be approximately 80 to hundreds darcy, allowing relatively unrestricted flow of fluid along the assemblies prior to remediation. This initial characterization of the full-scale test assemblies allowed a quantification of the permeability reduction following successive dents with the Casing Expander tool. Consequently, this study complements both systematic and detailed laboratory-scale studies of casing expansion (Kupresan et al., 2014; Radonjic and Kupresan, 2014; Wolterbeek et al., 2021b), and field trials (Wolterbeek et al., 2021b; Green et al., 2021).

Our study showed that even a single dent, set with a degree of inner casing expansion that is suitable in comparison to the initial cement quality, can reduce the permeability by multiple orders of magnitude, reaching values less than 1 mD when tested with water and at severe differential pressures. More representative, long-term gas testing with approximately 25 bar pressure difference resulted in a permeability of about 0.9 μD for a single dent in assembly A2 (A2-4). The gas permeabilities of several other sets of dents (A2-2, A2-3 and C6-3) were found to be too low for quantitative measurement. These observations agree with previous laboratory experiments of Kupresan et al. (2014), and Wolterbeek et al. (2021b), where casing expansion was found to decrease annular permeabilities by orders of magnitude, or even below the detection limit. Elimination of fluid migration in wells has also been found during recent onshore field trials (Wolterbeek et al., 2021b; Green et al., 2021).

The greater permeability reductions are observed for the larger degrees of casing expansion, which intuitively should improve the

mechanical bond between cement and casing, and lead to a certain compaction and densification of the cement. The vast majority of the permeability reduction occurred immediately upon placement of the first dent. The study has shown the effectiveness of casing expansion technology in treating even millimeter-sized channels located at the opposite interface of the casing that is being expanded. Qualitative findings suggest that even voids with gap sizes larger than 10 millimeters can be compacted and regain a level of cohesion, provided that a sufficient degree of expansion is imposed on the inner casing. When assessing the affected cement using Vickers hardness test, results suggest that the increase in hardness is connected with the level of compaction of the annular cement sheath. Within the set of dents A2-1, where less casing expansion was generated, the cement hardness was lower, suggesting deformation but not compaction of the cement. In sets of dents with more significant expansion and corresponding compaction of the cement, such as C6-3 and A2-4, a trend toward increased hardness was observed. Vickers hardness testing of casing steel indicated no significant changes in hardness at the dent locations compared to average hardness values away from these points.

Annular migration remediation by casing expansion technologies relies on the fascinating abilities of cement to deform and yield whilst confined. The current study has analyzed the possibility of closing relatively large channels in the annulus between casings. Future work should seek to further understand the stress–strain behavior and displacement properties of cement under such effectively confined conditions. Further studies could also address cases with a softer confining material, such as a weak formation, in order to both establish practical limitations and also new opportunities for expansion technologies.

CRediT authorship contribution statement

K. Beltrán-Jiménez: Methodology, Investigation. **H.J. Skadsem:** Conceptualization, Formal analysis, Visualization, Writing – original draft, Writing – review & editing. **J.K. Sunde:** Methodology, Investigation, Formal analysis, Visualization. **D. Gardner:** Methodology, Resources. **T.K.T. Wolterbeek:** Methodology, Investigation, Writing – original draft. **E.K. Cornelissen:** Conceptualization, Resources, Supervision. **W.J.G. Keultjes:** Resources, Supervision.

Declaration of competing interest

The authors declare that they have no known competing financial interests or personal relationships that could have appeared to influence the work reported in this paper.

Acknowledgments

Ullrigg Test Centre is acknowledged for facilitating and executing the Local Expander remediation experiment. In particular Ronny Håland, Arne Haaverstein and Stig Lomeland are acknowledged for their contributions to the experiment.

The Research Council of Norway, the Petroleum Safety Authority Norway, AkerBP, ConocoPhillips, Petrobras, Shell and Total are acknowledged for financing the work through PETROMAKS2 project number 308767/E30 and the P&A Innovation Program - a program for accelerating P&A technology development.

References

Anwar, I., Hatambeigi, M., Chojnicki, K., Taha, M.R., Stormont, J.C., 2021. Alteration in micro-mechanical characteristics of wellbore cement fracture surfaces due to fluid exposure. J. Pet. Sci. Eng. 205, http://dx.doi.org/10.1016/j.petrol.2021.108935.

Bittleston, S., Guillot, D., 1991. Mud removal: Research improves traditional cementing guidelines. Oilfield Rev. 44–54.

Bois, A.-P., Garnier, A., Rodot, F., Saint-Marc, J., Aimard, N., 2011. How to prevent loss of zonal isolation through a comprehensive analysis of microannulus formation. SPE Drill. Complet. 26 (01), 13–31.

Brufatto, C., Cochran, J., Conn, L., Power, D., El-Zeghaty, S., Fraboulet, B., Griffin, T., James, S., Munk, T., Justus, F., Levine, J., Montgomery, C., Murphy, D., Pfeiffer, J., Pornpoch, T., Rishmani, L., 2003. From mud to cement - building gas wells. Oilfield Rev. 15, 62–76.

Carter, G., Slagle, K., 1972. A study of completion practices to minimize gas communication. J. Pet. Technol. 24, 1170–1174. http://dx.doi.org/10.2118/3164-PA, SPE-3164-PA.

Constantinides, G., Ulm, F.-J., 2004. The effect of two types of c-s-h on the elasticity of cement-based materials: Results from nanoindentation and micromechanical modeling. Cem. Concr. Res. 34 (1), 67–80. http://dx.doi.org/10.1016/S0008-8846(03)00230-8.

Cornelissen, E.K., 2019. Method for sealing cavities in or adjacent to a cured cement sheath surrounding a well casing. US 2019/0264547 A1.

Cowan, M., 2007. Field study results improve squeeze cementing success. In: SPE Oklahoma City Oil and Gas Symposium/Production and Operations Symposium. pp. 1–8. http://dx.doi.org/10.2118/106765-MS, SPE-106765-MS.

Davies, R.J., Almond, S., Ward, R.S., Jackson, R.B., Adams, C., Worrall, F., Herringshaw, L.G., Gluyas, J.G., Whitehead, M.A., 2014. Oil and gas wells and their integrity: Implications for shale and unconventional resource exploitation. Mar. Pet. Geol. 56, 239–254. http://dx.doi.org/10.1016/j.marpetgeo.2014.03.001.

Du, H., Guo, R., Radonjic, M., 2015. Microstructure and micromechanics of wellbore cements under compression and thermal loading. In: U.S. Rock Mechanics/Geomechanics Symposium. pp. 1–11, ARMA-2015-498.

Frech-Baronet, J., Sorelli, L., Charron, J.-P., 2017. New evidences on the effect of the internal relative humidity on the creep and relaxation behaviour of a cement paste by micro-indentation techniques. Cem. Concr. Res. 91, 39–51. http://dx.doi.org/10.1016/j.cemconres.2016.10.005.

Goodwin, K.J., Crook, R.J., 1992. Cement sheath stress failure. SPE Drill. Eng. 7 (4), 291–296.

Green, C., Evans, R., Fry, B., Wruck, W.S., 2021. New technology closes micro-annular flow paths in the wellbore, stopping downhole gas from escaping to the surface. In: SPE/AAPG/SEG Unconventional Resources Technology Conference. pp. 1–9. http://dx.doi.org/10.15530/urtec-2021-5520.

Handin, J., 1965. Strength of oil well cements at downhole pressure-temperature conditions. SPE J. 5 (4), 341–347. http://dx.doi.org/10.2118/1300-PA, SPE-1300-PA.

Igarashi, S., Bentur, A., Mindess, S., 1996. Microhardness testing of cementitious materials. Adv. Cem. Based Mater. 4 (2), 48–57. http://dx.doi.org/10.1016/S1065-7355(96)90051-6.

Jackson, P., Murphey, C., 1993. Effect of casing pressure on gas flow through a sheath of set cement. In: SPE/IADC Drilling Conference and Exhibition. pp. 1–10. http://dx.doi.org/10.2118/25698-MS, SPE-25698-MS.

Justnes, H., van Loo, D., Reyniers, B., Skalle, P., Sveen, J., Sellevold, E.J., 1995. Chemical shrinkage of oil well cement slurries. Adv. Cem. Res. 7 (26), 85–90. http://dx.doi.org/10.1680/adcr.1995.7.26.85.

Kupresan, D., Heathman, J., Radonjic, M., 2014. Casing expansion as a promising solution for microannular gas migration. SPE Drill. Complet. 29 (04), 366–371.

Liu, J., Zeng, Q., Xu, S., 2020. The state-of-art in characterizing the micro/nano-structure and mechanical properties of cement-based materials via scratch test. Constr. Build. Mater. 254, 119255. http://dx.doi.org/10.1016/j.conbuildmat.2020.119255.

McLean, R.H., Manry, C.W., Whitaker, W.W., 1967. Displacement mechanics in primary cementing. J. Pet. Technol. 19, 251–260. http://dx.doi.org/10.2118/1488.

Nelson, E.B., Guillot, D., 2006. Well Cementing, second ed. Schlumberger, Sugar Land, Texas, US.

Oliver, W., Pharr, G., 1992. An improved technique for determining hardness and elastic modulus using load and displacement sensing indentation experiments. J. Mater. Res. 7 (6), 1564–1583. http://dx.doi.org/10.1557/JMR.1992.1564.

Parcevaux, P.A., Sault, P.H., 1984. Cement shrinkage and elasticity: A new approach for a good zonal isolation. In: SPE Annual Technical Conference and Exhibition, Houston, Texas. pp. 1–12. SPE-13176-MS. https://doi.org/10.2118/13176-MS.

Pedrosa, H.C., Reales, O.M., Reis, V.D., das Dores Paiva, M., Fairbairn, E.M.R., 2020. Hydration of portland cement accelerated by c-s-h seeds at different temperatures. Cem. Concr. Res. 129, http://dx.doi.org/10.1016/j.cemconres.2020.105978.

Radonjic, M., Kupresan, D., 2014. Mechanical expansion of steel tubing as a solution to leaky wellbores. J. Vis. Exp. 93, 52098. http://dx.doi.org/10.3791/52098.

Radonjic, M., Kupresan, D., Du, H., Olabode, A., 2015. Microstructures and micromechanics of wellbore cement under compression, in: The 13th International Congress on Rock Mechanics. pp. 1–12.

Roylance, D., 1996. Mechanics of Materials. John Wiley & Sons.

Sabins, F.L., 1990. Problems in cementing horizontal wells. J. Pet. Technol. 42, 398–400.

Sabins, F.L., Sutton, D.L., 1991. Interrelationship between critical cement properties and volume changes during cement setting. SPE Drill. Eng. 6, 88–94, SPE-20451-PA.

Sakai, Y., Nakatani, M., Takeuchi, A., Omorai, Y., Kishii, T., 2016. Mechanical behavior of cement paste and alterations of hydrates under high-pressure triaxial testing. J. Adv. Concr. Technol. 14 (1), 1–12. http://dx.doi.org/10.3151/jact.14.1.

Skadsem, H.J., Kragset, S., Sørbø, J., 2019. Cementing an irregular annulus geometry: Full-scale experiments and 3D simulations. In: SPE/IADC International Drilling Conference and Exhibition. The Hague, The Netherlands, pp. 1–15, SPE/IADC 194091.

Smith, R.L., Sandly, G.E., 1922. An accurate method of determining the hardness of metals, with particular reference to those of a high degree of hardness. Proc. Inst. Mech. Eng. 102 (1), 623–641. http://dx.doi.org/10.1243/PIME_PROC_1922_102_033_02.

Tao, C., Rosenbaum, E., Kutchko, B.G., Massoudi, M., 2021. A brief review of gas migration in oilwell cement slurries. Energies 14 (9), http://dx.doi.org/10.3390/en14092369.

Vignes, B., Aadnøy, B.S., 2010. Well-integrity issues offshore norway. SPE Prod. Oper. 25 (2), 145–150.

Wang, D., Zhao, Q., Zhang, J., Jin, L., 2019. Experimental research for elastic modulus of cement paste at ultra-early age based on indentation technique. Constr. Build. Mater. 226, http://dx.doi.org/10.1016/j.conbuildmat.2019.07.192.

Watson, T.L., Bachu, S., 2009. Evaluation of the potential for gas and CO_2 leakage along wellbores. SPE Drill. Complet. 24 (1), 115–126.

Webster, W., Eikerts, J., 1979. Flow after cementing: A field and laboratory study. In: SPE Annual Technical Conference and Exhibition. pp. 1–8. http://dx.doi.org/10.2118/8259-MS, SPE-8259-MS.

White, F.M., 1991. Viscous Fluid Flow, second ed. McGraw-Hill, Inc..

Wolterbeek, T., Cornelissen, E., Hangx, S., Spiers, C., 2021a. Impact of downhole pressure and fluid-access on the effectiveness of wellbore cement expansion additives. Cem. Concr. Res. 147, 106514. http://dx.doi.org/10.1016/j.cemconres.2021.106514.

Wolterbeek, T.K., Cornelissen, E.K., Nolan, S., Todea, F., Stam, W., Roggeband, S.M., Dam, L., van Riet, E.J., Ruckert, F., Keultjes, W.J.G., 2021b. Restoration of annular zonal isolation using localized casing expansion (LCE) technology: A proof of concept based on laboratory studies and field trial results. J. Pet. Sci. Eng. 197, 108103. http://dx.doi.org/10.1016/j.petrol.2020.108103, 1–28.

Zhang, M., Bachu, S., 2011. Review of integrity of existing wells in relation to CO_2 geological storage: What do we know? Int. J. Greenh. Gas Control 5, 826–840.

Zhang, H., Šavija, B., Schlangen, E., 2018. Combined experimental and numerical study on micro-cube indentation splitting test of cement paste. Eng. Fract. Mech. 199, 773–786. http://dx.doi.org/10.1016/j.engfracmech.2018.04.018.